

# Accumulation of opposite spins on the transverse edges of a two-dimensional electron gas in a longitudinal electric field

Yanxia Xing,<sup>1</sup> Qing-feng Sun,<sup>1,\*</sup> Liang Tang,<sup>2</sup> and JiangPing Hu<sup>2,†</sup>

<sup>1</sup>Beijing National Laboratory for Condensed Matter Physics and Institute of Physics, Chinese Academy of Sciences, Beijing 100080, People's Republic of China

<sup>2</sup>Department of Physics, Purdue University, West Lafayette, Indiana 47907, USA

(Received 24 April 2006; revised manuscript received 20 July 2006; published 16 October 2006)

We show that the spin-orbit interaction induced by the boundary-confining potential causes opposite spin accumulations on the transverse edges in a zonal two-dimensional electron gas in the presence of an external longitudinal electric field. While the bias is reversed, the spin-polarized direction is also reversed. The intensity of the spin accumulation is proportional to the bias voltage. In contrast to the bulk extrinsic and intrinsic spin-Hall effects, the spin accumulation by the confining potential is almost unaffected by impurity and survives even in strong disorder. The result provides a different mechanism to explain the recent experimental data.

DOI: 10.1103/PhysRevB.74.155313

PACS number(s): 72.25.-b, 85.30.Hi, 85.75.-d

## I. INTRODUCTION

Recently, two experimental groups observed the transverse opposite-spin accumulations near two edges of their devices in the presence of a longitudinal voltage bias.<sup>1,2</sup> One experiment is on a *n*-type GaAs's bar with a size of about  $300 \mu\text{m} \times 77 \mu\text{m}$ ,<sup>1</sup> and the spin accumulation is detected by Kerr-rotation spectroscopy. The other experiment is on a coplanar *p*-*n* junction light-emitting diode device.<sup>2</sup> Under a longitudinal bias, a circular polarization of the emitting light on two edges is detected. The directions of the polarization are opposite on the two edges, which suggests opposite spin accumulation on the two edges. Moreover, when the bias is reversed, the spin accumulations are reversed in the above two experiments.

These experiments were originally motivated to measure the predicted effects: the extrinsic and intrinsic spin-Hall effects (SHEs). The extrinsic SHE was discovered about a few decades ago,<sup>3,4</sup> and it originated from the spin-dependent scattering that deflected the spin-up and spin-down carriers towards the opposite edges of a sample. The intrinsic SHE is predicted first by Murakami *et al.* and Sinova *et al.* in a Luttinger spin-orbit- (SO) coupled three-dimensional (3D) *p*-doped semiconductor<sup>5</sup> and a Rashba SO-coupled two-dimensional electron gas<sup>6</sup> (2DEG), respectively. Recently, a number of sequential works have focused on this interesting effect.<sup>7-10</sup> Nonetheless, the intrinsic SHE still remains a controversial topic. The intrinsic spin-Hall conductivity was originally pointed out to be universal in the clean bulk sample.<sup>6</sup> However, some works have showed that the spin-Hall conductivity depends on the SO-coupling strength and electron Fermi energy in general.<sup>7</sup> Moreover, it has been shown recently that the impurity plays an important role on the intrinsic SHE. In an infinite system, the spin-Hall conductivity is found to be very sensitive to disorder,<sup>8</sup> and the effect vanishes even in a very weak disorder limit when the vertex correction is considered. While in a finite mesoscopic ballistic system, the SHE can survive.<sup>9</sup> The SHE and spin accumulations have been studied in the dirty or clean finite mesoscopic samples using the Landauer-Büttiker formalism

and the tight-binding Hamiltonian.<sup>11</sup> These works show that the opposite spin accumulations can be indeed generated on the two transverse edges in the finite system, and the SHE still presents below a critical disorder threshold.<sup>9</sup>

Although the spin accumulation observed in the two experiments appears to reflect the physics of the SHE, there is still a significant challenge to explain the observed experiment effect. The spin accumulation contributed from the extrinsic SHE has been shown to have the directions of spin polarization that are opposite to the experimental results.<sup>8</sup> While the intrinsic SHE is predicted to have the same directions of spin polarization as that observed in the experiments, it is expected to be scaled with length and eventually be vanished in Rashba SO-coupling systems in the presence of disorder. Since the experiments are not done in the ballistic region and the signal of spin accumulation has little dependence on the transversal length of the sample, it is not clear how the intrinsic SHE explains all experimental results solely.

In this paper, we give a new mechanism that can generate the opposite spin accumulations in two edges under the longitudinal (along the *x* direction) voltage bias. We first show the principle of this new mechanism. Considering an infinite zonal 2DEG with a confining potential in the *y* direction (see the inset of Fig. 1), which is described by the Hamiltonian  $H = \frac{p_x^2 + p_y^2}{2m^*} + V(y)$ , where  $p_{x/y}$  is the momentum operator and  $m^*$  is the effective mass of electrons.  $V(y)$  is the confining potential energy, which is constant in the center and quickly

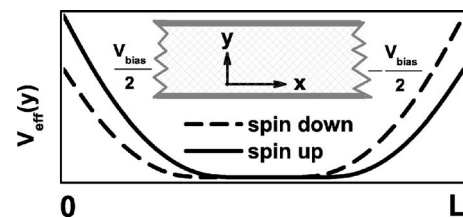


FIG. 1. Schematic diagram for the transverse-effective potential  $V_{\text{eff}}(y)$  in the zonal 2DEG for the positive  $+p_x$ . The inset is a schematic diagram for the infinite zonal 2DEG device.

increases near the edge. Based on the relativity effect, in the presence of the internal electric field  $\mathbf{E}=\nabla V(y)/e$ , there is a natural SO-coupling term  $V_{SO}=\frac{e\hbar}{2m^*c^2}\sigma_z(\mathbf{E}\times\mathbf{p})$ .<sup>12,13</sup> Considering the corresponding electric field  $\mathbf{E}=\nabla V(y)/e$  is perpendicular to the edge (along the  $x$  direction), only the element  $E_y$  of the  $y$  direction is nonzero and the SO-coupling energy reduces into  $V_{SO}=-\frac{\hbar}{2m^*c^2}\sigma_z p_x \frac{d}{dy}V(y)$ . So for the spin-down ( $\sigma_z=\downarrow$  or  $-1$ ) electrons, its effective potential  $V_{eff}(y)=V(y)+V_{SO}(y)$  is lower than the one of spin-up electrons at the edge of  $y=0$  for positive  $+p_x$  (see Fig. 1). On the other hand, at the other edge of  $y=L$ , the effective potential  $V_{eff}$  of the spin-up electrons is lower for  $+p_x$  (see Fig. 1). Thus, the spin accumulations near the two transverse edges (at  $y=0$  and  $y=L$ ) are formed when electrons occupy the positive  $+p_x$  states under the positive longitudinal (along the  $x$  direction) bias. When the bias is reversed, the electrons occupy the negative  $-p_x$  state and the spin accumulation reverses its sign. Therefore it produces the same spin accumulation as observed in the experiments.<sup>2</sup> In the present model, the spin accumulation completely originates from the structure-confining potential, so it is not affected by the impurity and the dephase. In a word; the structure-confining potential can also induce the opposite spin accumulation, which can be the origin of the experimentally observed spin accumulation.

The paper is organized as follows: in Sec. II, we will mention and solve the model in detail. The results and discussions are in Sec. III. Finally, a brief summary is given in Sec. IV.

## II. MODEL AND SOLUTION

The Hamiltonian of the zonal 2DEG can be written as

$$H = \frac{p_x^2 + p_y^2}{2m^*} + V(y) - \frac{\hbar}{2m^*c^2}\sigma_z p_x \frac{d}{dy}V(y). \quad (1)$$

Here the first term is kinetic energy, the second term is the potential energy, and the third term comes from the SO-coupling energy due to the boundary-confining potential  $V(y)$  as mentioned in the Introduction.

Due to the fact  $[p_x, H]=0$  and  $[\sigma_z, H]=0$ ,  $k_x$  and  $\sigma_z$  are the good quantum numbers, the eigenstates in such a structure can be written in the form  $\Psi(x, y) = \phi_{nk_x}(y)\exp(ik_x x)$  with the dispersion relation  $E = \epsilon_{nk_x} + \hbar^2 k_x^2 / 2m^*$ . The index  $n$  numbers the different subbands with the wave function  $\phi_{nk_x}(y)$  in the  $y$  direction and energy  $\epsilon_{nk_x}$ , which are functions of the wave vector  $k_x$ . The transverse wave function  $\phi_{nk_x}(y)$  satisfies the equation

$$\left[ \frac{p_y^2}{2m^*} + V(y) - \gamma\sigma_z \frac{dV(y)}{dy} \right] \phi_{nk_x}(y) = \epsilon_{nk_x} \phi_{nk_x}(y), \quad (2)$$

where  $\gamma = \frac{\hbar^2 k_x}{2m^*c^2}$ . In the experiment, the length  $L$  along the transverse  $y$  direction is very long [e.g., in the order of tens of micron in Ref. 1] while the confining potential is only limited in several atom's layers. So we model this potential  $V(y)$  as a square potential well, i.e.,  $V(y)=0$  for  $0 < y < L$  and  $V(y)=V$  for others  $y$ . In this case,  $V_{SO} = -\gamma\sigma_z \frac{d}{dy}V(y)$  becomes

the  $\delta$  function. The Hamiltonian can be solved analytically, and the Schrödinger equation [Eq. (2)] for the spin-up electron reduces into

$$\left[ \frac{p_y^2}{2m^*} + V(y) + \gamma V[\delta(y) - \delta(y-L)] \right] \phi(y) = \epsilon \phi(y). \quad (3)$$

The spin-down electronic Schrödinger equation is similar to Eq. (3) except  $\gamma \rightarrow -\gamma$ . The wave function  $\phi(y)$  in Eq. (3) can be written as

$$\phi(y) = \begin{cases} Ae^{\beta y}, & y < 0 \\ \sin(k_y y + \theta), & 0 < y < L \\ Be^{-\beta y}, & y > L, \end{cases} \quad (4)$$

where  $k_y = \sqrt{2m^* \epsilon} / \hbar$ ,  $\beta = \sqrt{2m^*(V - \epsilon)} / \hbar$ , and  $A$ ,  $B$ , and  $\theta$  are the constants to be determined by the boundary conditions. Here the boundary conditions are  $\phi(y)|_{y=0^-} = \phi(y)|_{y=0^+}$  and  $\phi'(y)|_{y=0^+} - \phi'(y)|_{y=0^-} = \pm(2m^* \gamma / \hbar^2) \phi(y)|_{y=0}$ , which lead to

$$\sin \theta = A,$$

$$\sin(k_y L + \theta) = Be^{-\beta L},$$

$$k_y \cos \theta - A\beta = 2m^* \gamma A,$$

$$\beta Be^{-\beta L} + k_y \cos(k_y L + \theta) = 2m^* \gamma Be^{-\beta L}.$$

Solving the equation set, we get  $A$ ,  $B$ ,  $\theta$ ,  $k_y$ , and consequently  $\epsilon_{nk_x}$  and  $\phi_{nk_x}(y)$ . Then the spin-up electron-probability distribution  $P_{nk_x, \uparrow}(y) = |\phi_{nk_x}(y)|^2$  is obtained. The same calculation can be done for the spin-down electron. Due to the system being universal along the  $x$  direction, and the spin accumulation being independent of  $x$ ,  $P_{nk_x, \uparrow \downarrow}(y)$  completely describes spin distribution.

Although the wave function of the square confining potential  $V(y)$  model can be expressed in analytical form, it does not describe the real system in which the potential is not abrupt and a gradual change from the bottom to top close to the interface is expected. For this reason, we consider the real parabolic confining potential  $V(y)$  and solve the system numerically by using the tight-binding Hamiltonian.<sup>11</sup> In addition, we also study the disorder effect on the spin accumulations. In the tight-binding approximation, the Hamiltonian in Eq. (2), which is related to the  $y$  direction, can be written as the following discrete lattice version:

$$H = \sum_{i, \sigma} (\epsilon_i + V_i + \sigma_z V_{SO, i}) a_{i\sigma}^\dagger a_{i\sigma} + \sum_{\langle ij \rangle, \sigma} t a_{i\sigma}^\dagger a_{j\sigma}, \quad (5)$$

where  $i$  is the site index along the  $y$  direction,  $\sigma = \uparrow, \downarrow$  (or  $\pm 1$ ) is the spin index in the  $z$  direction, and  $t = \hbar^2 / 2m^* a^2$  represents the hopping matrix element with the lattice constant  $a$ . The confining potential  $V(y)$  is assumed to be parabolic:  $V(y) = V \frac{(y-6a)^2}{25a^2}$  for  $a \leq y \leq 5a$ ,  $V(y) = 0$  for  $5a < y \leq L - 5a$ , and  $V(y) = V \frac{(y-L+5a)^2}{25a^2}$  for  $L - 5a < y \leq L$ . For a clean system, the onsite energy  $\epsilon_i = 0$ , and  $\epsilon_i$  is randomly distributed between  $[-W/2, W/2]$  for the dirty system. The Hamiltonian in Eq. (5) can be easily solved by numerically calculating the

eigenvalues and eigenstates of the Hamiltonian matrix. Due to the decoupling between the different spin states in the Hamiltonian, we can solve the eigenvalues and eigenwave functions separately for the spin-up and spin-down electrons, whereafter the spin-up and spin-down electron probability distribution  $P_{nk_x\sigma}(i)$  in the subband  $n$  and the longitudinal momentum  $\hbar k_x$  is obtained straightforwardly.

While the longitudinal bias is zero, the spin accumulation  $S(y)$  is zero everywhere, because of the existence of the time-reversal invariance. On the other hand, when a bias  $V_{\text{bias}}$  is added, the spin accumulations  $S(y)$  will emerge. Considering the device under the positive bias  $V_{\text{bias}}$  and at the zero temperature, the  $+k_x$  states with its energy between  $E_f - V_{\text{bias}}/2$  and  $E_f + V_{\text{bias}}/2$  are occupied by electrons, while the states for the negative  $-k_x$  are empty, here  $E_f$  is the Fermi energy. Then, under the small bias and taking the linear approximation, the spatial density distribution  $P_{\uparrow\downarrow}(i)$  of the spin-up (down) electrons along the  $y$  direction for the unit bias is  $P_{\uparrow\downarrow}(i) = \sum_n \rho_n(E_{k_x}) P_{nk_x,\uparrow\downarrow}(i)$ , where  $\rho_n(E_{k_x})$  is the density of state in the subbands  $n$  with  $E_{k_x} = E_f - \epsilon_{nk_x}$ , and the sum is over all subbands  $n$  whose cut-off energy is lower than  $E_f$ . The spin-accumulation density and charge density in the linear bias can be obtained as  $P_s(i) \equiv \lim_{V_{\text{bias}} \rightarrow 0} \frac{S(i)}{V_{\text{bias}}} = \frac{\hbar}{2} [P_{\uparrow}(i) - P_{\downarrow}(i)]$  and  $P_e(i) = e[P_{\uparrow}(i) + P_{\downarrow}(i)]$ .

In the numerical calculation, we choose the realistic parameters as the ones in the experiment:<sup>14</sup> the electronic effective mass  $m^* = 0.05m_e$  and the Fermi energy  $E_f = 0.1$  eV, in which the corresponding electron concentration is approximately  $n_{2D} = 10^{12}$  cm<sup>-2</sup>. The energy unit is set to 1 eV, and the length unit is 1 nm for the analytic model, or 1 a.u. for the tight-binding model. The lattice constant  $a$  in the tight-binding model is around 0.196 nm.

### III. NUMERICAL RESULTS AND DISCUSSION

First, we study spin accumulation in the clean system. In the present system, the spin-accumulation density  $P_s(y)$  depends on the transverse position  $y$ , and it is independent of the longitudinal position  $x$ . Figures 2 and 3 show the spin-accumulation density  $P_s(y)$  and charge density  $P_e(y)$  versus  $y$  for the case of the square and the parabolic confining potential  $V(y)$ , respectively. First of all, the opposite spin accumulations polarized in the  $z$  direction are indeed generated near the two edges regardless of the square or the parabolic potential. If the bias is reversed, the electrons occupy the negative  $-k_x$  states instead of the positive  $+k_x$  states and the spin accumulations also are reversed. These results are consistent with the experimental results.<sup>1,2</sup> The opposite spin accumulations here obviously originate from the confining potential as mentioned in the Introduction because there is no other interaction except the potential  $V(y)$ . Second, the spin mainly accumulates near the two edges, and it is small and oscillates in the bulk. The oscillation is expected due to the existence of the Fermi surface. The period is given by  $2\pi/k_F$ . For a fixed Fermi energy (e.g.,  $E_f = 0.1$  eV), the wider the width  $L$  is, the more the subbands below  $E_f$  will be. At the same time, the oscillation times of  $P_s$  and  $P_e$  are more and the oscillation amplitudes are smaller. So the bulk  $P_s$

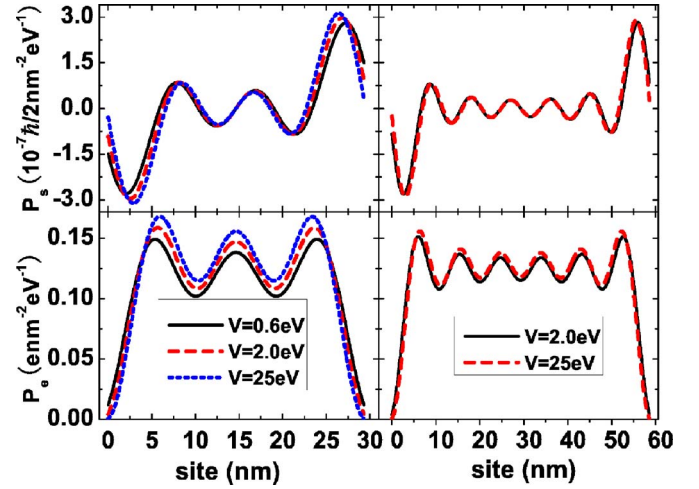


FIG. 2. (Color online) The transverse distribution of the spin and charge density,  $P_s(y)$  and  $P_e(y)$ , vs  $y$  for the square confining potential. Left panel:  $L=29.3$  nm, right panel:  $L=58.6$  nm. Notice that the two curves in the right panel almost overlap together so that they almost cannot be distinguished.

almost vanishes and  $P_e$  approaches a constant at large  $L$ . But the spin accumulations near the edge, including the intensity and the location, is almost independent with  $L$ . Third, we discuss the characters of the spin accumulations  $P_s(y)$  as a function of the strength  $V$  of the confining potential  $V(y)$ . The characters are slightly different for the square and parabolic potentials. When  $V=0$ ,  $P_s(y)=0$  for both the square and parabolic potentials. With increasing  $V$ ,  $P_s(y)$  emerges. For the square potential,  $P_s(y)$  quickly arises in the beginning. Around  $V=5E_f \approx 0.5$  eV,  $P_s(y)$  has reached a saturated value. Thereafter the value almost does not change with further increasing  $V$  [see Figs. 2(a) and 2(b)]. For the parabolic potential,  $P_s(y)$  increases slowly. Around  $V=8$  eV, it saturates. For comparison, we also show the charge density  $P_e(y)$

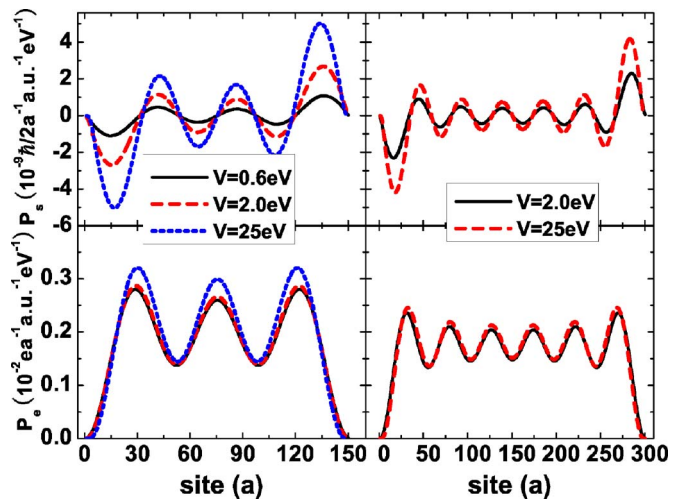


FIG. 3. (Color online) The transverse distribution of the spin and charge density,  $P_s(y)$  and  $P_e(y)$ , vs  $y$  for the parabolic confining potential. Left panel:  $L=150a$ , right panel:  $L=300a$ . Notice that the blue dashed curves in the below panel almost overlap perfectly with the black solid curves so that they almost cannot be seen.

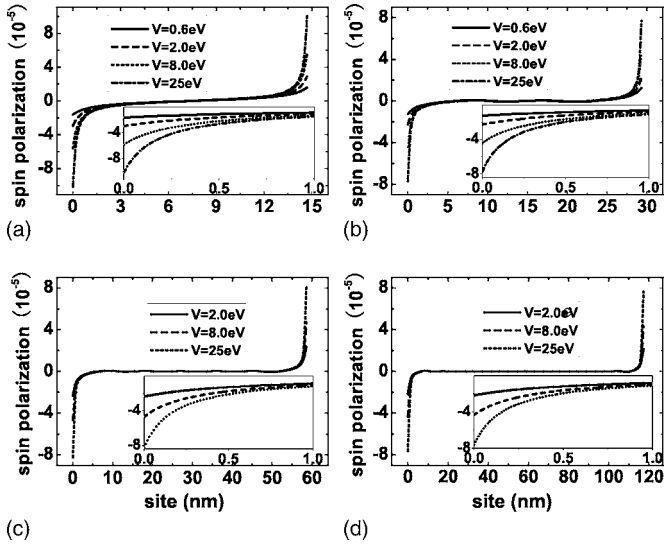


FIG. 4. The spin polarization  $P_s/P_e$  vs the transverse site  $y$  for the square confining potential. Panels (a),(b),(c),(d) correspond to  $L=14.6$  nm,  $L=29.3$  nm,  $L=58.6$  nm, and  $L=117.3$  nm, respectively. The insets show the detailed distribution near the edge of  $y=0$  in the central panel.

in Figs. 2 and 3. Here  $P_e(y) > 0$  in any position  $y$ , and  $P_e(y)$  is even symmetric while  $P_s(y)$  is odd symmetric.

Next, we discuss the spin polarization  $P_s(y)/P_e(y)$ . In the central panels of Figs. 4 and 5, we plot the transverse distribution of the spin polarization for the square and parabolic confining potential  $V(y)$ , respectively. It is clearly shown that the opposite spin polarization emerges on the transverse two edges wherever  $L$  is set. For example, in Figs. 4 and 5, the transverse width  $L$  is set to 14.6, 29.3, 58.6, and 117.3 nm, which is very different, but the spin-polarization distributions near the edge are almost identical. In addition, the spin po-

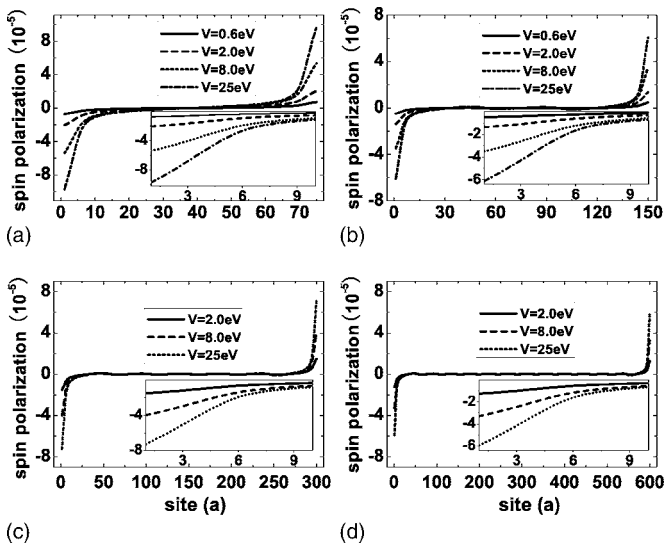


FIG. 5. The spin polarization  $P_s/P_e$  vs the transverse site  $y$  for the parabolic confining potential. Panels (a),(b),(c),(d) correspond to  $L=75a$ ,  $150a$ ,  $300a$ , and  $600a$ , respectively. The insets show the detailed distribution near the edge of  $y=0$  in the central panel.

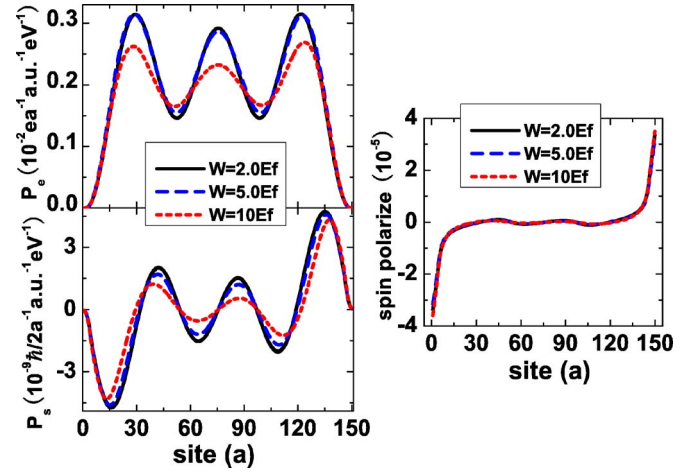


FIG. 6. (Color online) The charge-density distribution  $P_e$  (a), the spin-density distribution  $P_s$  (b), and the spin polarization  $P_s/P_e$  (c) vs the transverse site  $y$  for the different disorder  $W$ , respectively. The other parameters are  $E_f=0.1$  eV,  $L=150a$ , and  $V=8$  eV. Notice that the black solid curves and the blue dashed curves in the left panel almost overlap each other, and the three curves in the right panel also overlap perfectly, so that they almost cannot be distinguished.

larization on the transverse edge is close to a linear function as  $V$  while  $P_s(y)$  is hardly affected by the strength of  $V$  (see Figs. 2 and 3). The detailed distributions of the spin polarization near the edge of  $y=0$  are magnified and shown in the insets (in Figs. 4 and 5). The distribution range for the parabolic potential is slightly wider than that for the square potential because the variation range of the parabolic potential  $V(y)$  is wider than that of the square potential  $V(y)$ .

The above result is obtained in a clean system. In the following, we study the spin accumulation in the dirty system. Figure 6 displays the transverse distribution of  $P_s(y)$ ,  $P_e(y)$ , and spin polarization  $P_s(y)/P_e(y)$  with different disorder strength  $W=2E_f$ ,  $5E_f$ ,  $10E_f$ . In these calculations,  $P_s(y)$  and  $P_e(y)$  are obtained by averaging over up to 5000 realizations of disorder. From Fig. 6, we can see that the spin accumulation  $P_s(y)$  and the spin polarization near the two edges are almost unaffected by the disorder; even the disorder  $W$  is very strong (e.g.,  $W=10E_f$ ). In fact, the spin accumulation in the present device originates from the confining potential near the edge, where the effective potentials for spin-up and spin-down electrons are different (see Fig. 1). Intuitively, the spin polarization is expected to be unaffected by the disorder as well as the dephase. Additionally, with the increasing of the disorder  $W$ , the amplitudes of the oscillation of  $P_e(y)$  and  $P_s(y)$  in the bulk are slightly reduced (see left panels in Fig. 6), and their fluctuations are increased linearly (not shown).

To compare our numerical results with the experiment,<sup>1</sup> we calculate the value of spin polarization and accumulation in the experiment. From the experimental data, the spin density at the peak can be estimated:  $P_s \approx (1.5-4.2) \times 10^{-6} \text{ nm}^{-2} \text{ eV}^{-1}$ , and the spin polarization is  $(1.0-2.8) \times 10^{-4}$  for a thickness  $h=0.9 \mu\text{m}$ .<sup>15</sup> From figures (e.g., Figs. 2 and 4), our calculation shows that the peak spin density

$P_s \approx 0.3 \times 10^{-6} \text{ nm}^{-2} \text{ eV}^{-1}$  and the spin polarization is  $0.8 \times 10^{-4}$ . The value of the spin polarization is comparable with the experiment. Due to the big thickness in the experiment, the spin accumulation  $P_s$  in our calculation seems to be several times smaller than that of the experiment. In addition, it should be mentioned that the spin-relaxation length in our results are determined by  $1/k_F$ , which is about 10 nm (see Figs. 2 and 3). This relaxation length is in the same order of the one in the recent intrinsic spin-Hall effect.<sup>9</sup> However, it has quite a large discrepancy in comparison with the experimental results, in which the spin-relaxation length is about  $10 \mu\text{m}$ .<sup>1</sup> One possible reason for this discrepancy is the spin diffusion. In the experiment, the system is in the diffusive region, and the spin accumulation in the edges can diffuse towards the center. Then the spin-relaxation length is greatly lengthened, and it is determined by the spin-diffusion length. Indeed, a more precise quantitative calculation perhaps requires us to consider the spin-orbit coupling in the bulk and spin-diffusing effect at the boundary. However, our simple model indeed produces the same effect as well as the same order of magnitude as one measured in the experiments.

#### IV. CONCLUSION

In summary, we propose a different mechanism to explain the spin accumulations at the edges of a zonal two-

dimensional electron system. Due to the strong structure-confining potential in the boundary, the induced spin-orbit interaction leads to the opposite spin accumulation on the two transverse edges under the longitudinal voltage bias. The spin-polarized direction can be reversed while the bias is reversed. The intensity of the polarization is also proportional to the external longitudinal voltage bias. These results are consistent with the recent experiment, except that the spin-relaxation length has the large discrepancy, which possibly results from the the diffusion effect. Moreover, the experimental test of the new mechanism can be easily performed in future experiments. Unlike the extrinsic and intrinsic SHE, the spin accumulations in the present mechanism are hardly affected by the disorder and dephase, and can exist even in the strong disorder system.

*Note added in proof.* Recently, we noticed that Jiang and Hu also addressed a similar problem.<sup>16</sup>

#### ACKNOWLEDGMENTS

We gratefully acknowledge financial support from the Chinese Academy of Sciences and NSF-China under Grants No. 90303016, No. 10474125, and No. 10525418. L.T. and J.P.H. are also supported by NSF with award number PHY-0603759.

\*Electronic address: sunqf@aphy.iphy.ac.cn

<sup>†</sup>Electronic address: hu4@physics.purdue.edu

- <sup>1</sup>Y. K. Kato, R. C. Myers, A. C. Gossard, and D. D. Awschalom, *Science* **306**, 1910 (2004); V. Sih, R. C. Myers, Y. K. Kato, W. H. Lau, A. C. Gossard, and D. D. Awschalom, *Nat. Phys.* **1**, 31 (2005).
- <sup>2</sup>J. Wunderlich, B. Kaestner, J. Sinova, and T. Jungwirth, *Phys. Rev. Lett.* **94**, 047204 (2005).
- <sup>3</sup>M. I. Dyakonov and V. I. Perel, *JETP Lett.* **13**, 467 (1971); *Phys. Lett.* **35A**, 459 (1971).
- <sup>4</sup>J. E. Hirsch, *Phys. Rev. Lett.* **83**, 1834 (1999).
- <sup>5</sup>S. Murakami, N. Nagaosa, and S. C. Zhang, *Science* **301**, 1348 (2003); *Phys. Rev. B* **69**, 235206 (2004).
- <sup>6</sup>J. Sinova, D. Culcer, Q. Niu, N. A. Sinitsyn, T. Jungwirth, and A. H. MacDonald, *Phys. Rev. Lett.* **92**, 126603 (2004).
- <sup>7</sup>E. M. Hankiewicz, L. W. Molenkamp, T. Jungwirth, and J. Sinova, *Phys. Rev. B* **70**, 241301(R) (2004); B. K. Nikolić, L. P. Zárbo, and S. Souma, *ibid.* **72**, 075361 (2005); A. Reynoso, Gonzalo Usaj, and C. A. Balseiro, *ibid.* **73**, 115342 (2006).
- <sup>8</sup>J. I. Inoue, G. E. W. Bauer, and L. W. Molenkamp, *Phys. Rev. B* **70**, 041303(R) (2004); E. G. Mishchenko, A. V. Shytov, and B. I. Halperin, *Phys. Rev. Lett.* **93**, 226602 (2004).
- <sup>9</sup>J.-P. Hu, B. A. Bernevig, and C.-J. Wu, *Int. J. Mod. Phys. B* **17**, 5991 (2003); L. Sheng, D. N. Sheng, and C. S. Ting, *Phys. Rev. Lett.* **94**, 016602 (2005); L. Sheng, D. N. Sheng, C. S. Ting, and

- F. D. M. Haldane, *ibid.* **95**, 136602 (2005); C. P. Moca and D. C. Marinescu, *Phys. Rev. B* **72**, 165335 (2005); J. Li, L. Hu, and S.-Q. Shen, *ibid.* **71**, 241305(R) (2005); B. K. Nikolić, S. Souma, L. P. Zárbo, and J. Sinova, *Phys. Rev. Lett.* **95**, 046601 (2005); J. Yao and Z. Q. Yang, *Phys. Rev. B* **73**, 033314 (2006); J. Wang, K. S. Chan, and D. Y. Xing, *ibid.* **73**, 033316 (2006).
- <sup>10</sup>Y. Yao and Z. Fang, *Phys. Rev. Lett.* **95**, 156601 (2005); Z. F. Jiang, R. D. Li, S.-C. Zhang, and W. M. Liu, *Phys. Rev. B* **72**, 045201 (2005); O. Chalaev and D. Loss, *ibid.* **71**, 245318 (2005); B. A. Bernevig and S. C. Zhang, *Phys. Rev. Lett.* **95**, 016801 (2005); R. Raimondi and P. Schwab, *Phys. Rev. B* **71**, 033311 (2005).
- <sup>11</sup>Chapters 2 and 3, in *Electronic Transport in Mesoscopic Systems*, edited by S. Datta (Cambridge University Press, Cambridge, England 1995).
- <sup>12</sup>J. D. Bjorken and S. D. Drell, *Relativistic Quantum Mechanics* (McGraw-Hill, New York, 1965).
- <sup>13</sup>Q. F. Sun, J. Wang, and H. Guo, *Phys. Rev. B* **71**, 165310 (2005).
- <sup>14</sup>Y. S. Gui, C. R. Becker, N. Dai, J. Liu, Z. J. Qiu, E. G. Novik, M. Schäfer, X. Z. Shu, J. H. Chu, H. Buhmann, and L. W. Molenkamp, *Phys. Rev. B* **70**, 115328 (2004).
- <sup>15</sup>Notice that the spin polarization  $(1.0-2.8) \times 10^{-4}$  from the experimental data is the polarization  $(j_{\uparrow}-j_{\downarrow})/(j_{\uparrow}+j_{\downarrow})$  of the current, not  $(P_{\uparrow}-P_{\downarrow})/(P_{\uparrow}+P_{\downarrow})$ .
- <sup>16</sup>Y. J. Jiang and L. B. Hu, *Phys. Rev. B* **74**, 075302 (2006).